PERGAMON

International Journal of Heat and Mass Transfer 43 (2000) 2289–2301

International Journal of HEAT and MASS TRANSFER

www.elsevier.com/locate/ijhmt

Buoyant convection in a vertical cylinder with azimuthally-varying sidewall temperature

Kwang Hyo Chung[a], Jae Min Hyun[a,*], Hiroyuki Ozoe[b]

[a]*Department of Mechanical Engineering, Korea Advanced Institute of Science & Technology, 373-1 Kusong-dong, Yusong-gu, Taejon 305-701, South Korea*

[b]*Institute of Advanced Material Study, Kyushu University, Kasuga Koen 6-1, Kasuga 816, Japan*

Received 9 April 1999; received in revised form 24 September 1999

Abstract

A numerical investigation is made of three-dimensional natural convection of a Boussinesq-fluid in a vertically-mounted cylindrical container. The boundary conditions are such that the wall temperature θ_Σ is inhomogeneous in the horizontal azimuthal direction but increases in the vertical direction. Interest is confined to flows with globally-stable stratifications and with substantial azimuthal variations in thermal boundary conditions. Comprehensive numerical solutions to the Navier–Stokes equations are obtained. A variety of specific thermal boundary conditions are considered for detailed examination. Flow characteristics are described in broad ranges of principal nondimensional parameters, i.e., the vertical and horizontal Rayleigh numbers, the container aspect ratio and the Prandtl number. Three-dimensional flow patterns are constructed. For large Rayleigh numbers, the azimuthal inhomogeneity of boundary conditions is absorbed in the boundary layers. In the interior core, flow is determined mostly by the azimuthally-averaged temperature boundary condition. Exemplifications are made for two cases: (1) when θ_Σ is vertically uniform, and (2) when θ_Σ is a linear function of height. For both cases, the interior core is stably-stratified, and on the planes of constant height, horizontal motions are present. Vertical and horizontal profiles of major flow variables are plotted. The explicit effect of increasing the vertical gradient of θ_Σ on the global flow structure is delineated.

Keywords: Buoyant convection; Azimuthally-varying sidewall temperature; Vertical stratification

1. Introduction

Buoyant convection in an enclosure has been extensively studied. Interest is often confined to the situations in which the buoyant effect is significant such that the representative system Rayleigh number *Ra* is large. This implies that the entire flow field can be divided into thin boundary layers and a practically inviscid interior core. A canonical configuration is that of an incompressible Boussinesq-fluid in a two-dimensional rectangular cavity with different, but constant, temperatures at the two vertical sidewalls. The horizontal walls are insulated. The benchmark numerical solutions for a square cavity were published by Davis [1], and various issues beyond the above-stated fundamental flow model have been raised (see, e.g., [2]).

One key contention is the exploration of more

* Corresponding author. Tel.: +82-42-869-3012; fax: +82-42-869-3210.

E-mail address: jmhyun@cais.kaist.ac.kr (J.M. Hyun).

0017-9310/00/$ - see front matter
PII: S0017-9310(99)00308-7

Nomenclature

A	aspect ratio [$= H/R$]
g	gravitational acceleration
H	height of cylinder
n	frequency of sidewall boundary condition
p, P	dimensional, dimensionless pressures [$= pR^2/\rho\alpha^2$]
Pr	Prandtl number [$= \nu/\alpha$]
r	radial direction
R	radius of cylinder
Ra	overall Rayleigh number [$= g\beta\Delta TR^3/\nu\alpha$]
S_z	strength of vertical stratification
T	temperature
u, v, w	velocities in x, y and z directions
U, V, W	dimensionless velocities in x, y and z directions [$= uR/\alpha$, vR/α, wR/α]
x, y, z	coordinates
X, Y, Z	dimensionless coordinates [$= x/R$, y/R, z/R]

Greek symbols

α	thermal diffusivity
β	volumetric expansion coefficient
ΔT	temperature difference [$= (T_{\max} - T_{\min})_{\text{topwall}}$]
ν	kinematic viscosity
ϕ	horizontal angle (azimuthal angle)
ρ	density
T_0	reference temperature [$= (T_{\max} + T_{\min})_{\text{topwall}}/2$]
θ	dimensionless temperature [$= (T - T_0)/\Delta T$]

Subscripts

max	maximum quantities
min	minimum quantities
h	horizontal direction
Σ	sidewall
top	top wall
v	vertical direction
0	reference

realistic three-dimensional features. For example, Refs. [3–6] considered a cubical box in which the flow is maintained by different, but constant temperatures at the vertical walls. Refs. [7–10] reported in general three-dimensional flow features for cylindrical containers. These preceding investigations revealed the global flow patterns and heat transfer characteristics of buoyancy-influenced convection in three-dimensional containers. It is noted that buoyant convection in an enclosure is extremely sensitive to the character and manner in which the boundary conditions are imposed upon the system. Therefore, any findings of the previous research should be viewed with caution since the results are specific to the geometry and boundary conditions adopted in those particular problem settings.

In this paper, efforts are directed towards delineating the three-dimensional flow field when there exist distinct azimuthal nonuniformities in the thermal boundary conditions of a vertically-mounted cylindrical enclosure. In the present setup, the boundary temperature profiles on the cylindrical sidewall are gravitationally stable, i.e., the boundary temperature increases with height. However, flow is generated by a continuous variation of boundary temperature in the azimuthal direction in a given horizontal plane. As emphasized earlier, the system-wide Rayleigh number for the whole container is large, and, accordingly, a boundary-layer-type flow prevails in the cylinder. The main question is the flow behavior in the boundary layers and in the interior which are initiated by the azimuthal nonuniformity of thermal boundary condition.

The present flow configuration is relevant to industrial applications. An example can be found in a cylindrical fuel tank when the sidewall temperature has azimuthal variations due to the oblique insolation. Also, the present problem statement has implications for the practical arrangement of growing high-quality crystals. In realistic situations, the presence of azimuthal variations of thermal boundary conditions is inevitable, and the transport phenomena should be determined in accordance with these imposed conditions.

A literature survey indicates that several prior investigations dealt with the aspects of three-dimensional flows in an enclosure. Jischke and Doty [11] pursued analytical methods to obtain solutions for unsteady buoyant convection under gravitationally-stable thermal boundary conditions. A classical modified asymptotic expansion scheme was utilized, and the boundary layer–inviscid interior coupling was exploited. The resulting analytical solutions disclosed salient characteristics in the interior for large Ra and for the Prandtl number $Pr \sim O(1)$. Crespo and Bontoux [12] studied the development of non-axisymmetric flows in an axisymmetric cylinder heated at the bottom. The issue of azimuthal dependence of temperature field was discussed by several authors [13–18], principally in the context of designing a crystal-growing furnace and attendant technological apparatus.

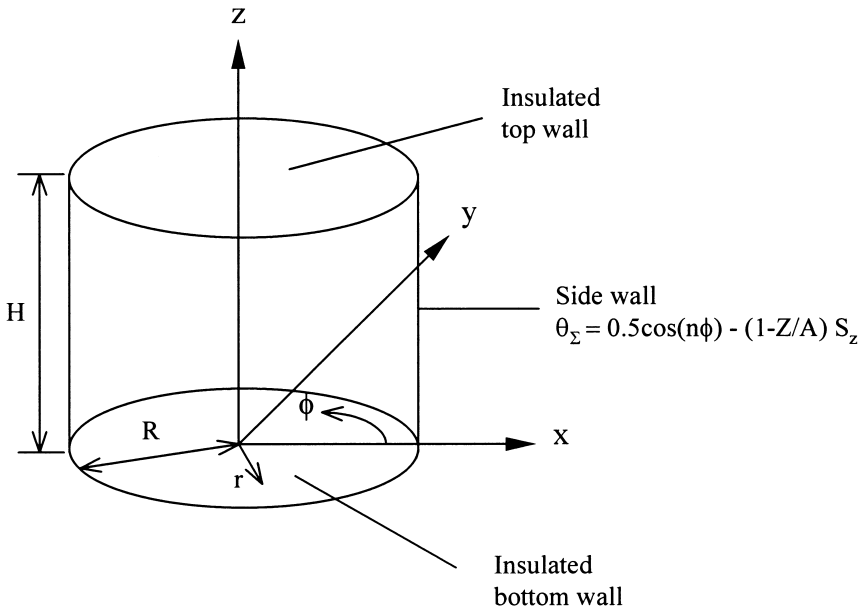

Fig. 1. Flow configuration and coordinates.

The objective of this paper is to conduct comprehensive and systematically-organized numerical computations of fully-three-dimension flows in a vertically-mounted cylinder. The velocity and temperature data in the entire region of the cylinder will be scrutinized, and important parameters will be identified. The explicit influence of horizontal non-uniformity of the sidewall condition on the prominent flow characteristics will be examined.

2. The flow model

An incompressible fluid is contained in a vertically-mounted closed cylindrical vessel (radius R, height H, aspect ratio $A \equiv H/R$), as sketched in Fig. 1. For a Boussinesq-fluid, the properly-nondimensionalized governing equations, using the coordinates (x, y, z) with corresponding velocity components (u, v, w), read

$$\frac{\partial U}{\partial X} + \frac{\partial V}{\partial Y} + \frac{\partial W}{\partial Z} = 0 \tag{1}$$

$$U\frac{\partial U}{\partial X} + V\frac{\partial U}{\partial Y} + W\frac{\partial U}{\partial Z} = -\frac{\partial P}{\partial X} + Pr\nabla^2 U \tag{2}$$

$$U\frac{\partial V}{\partial X} + V\frac{\partial V}{\partial Y} + W\frac{\partial V}{\partial Z} = -\frac{\partial P}{\partial Y} + Pr\nabla^2 V + Ra \cdot Pr \cdot \theta \tag{3}$$

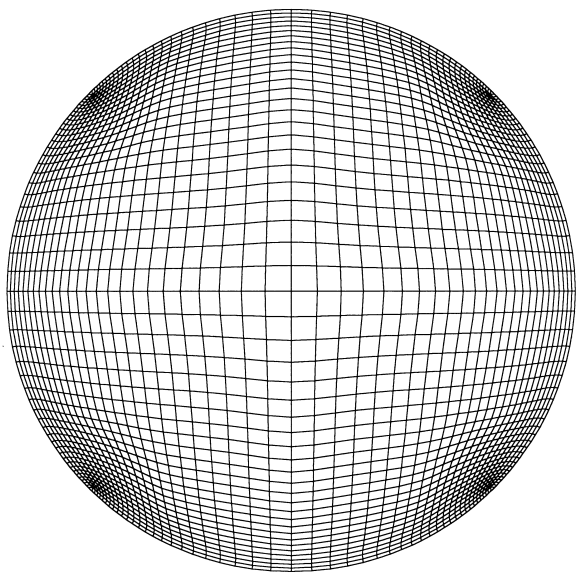

Fig. 2. (52 × 52) grid network in the x–y plane.

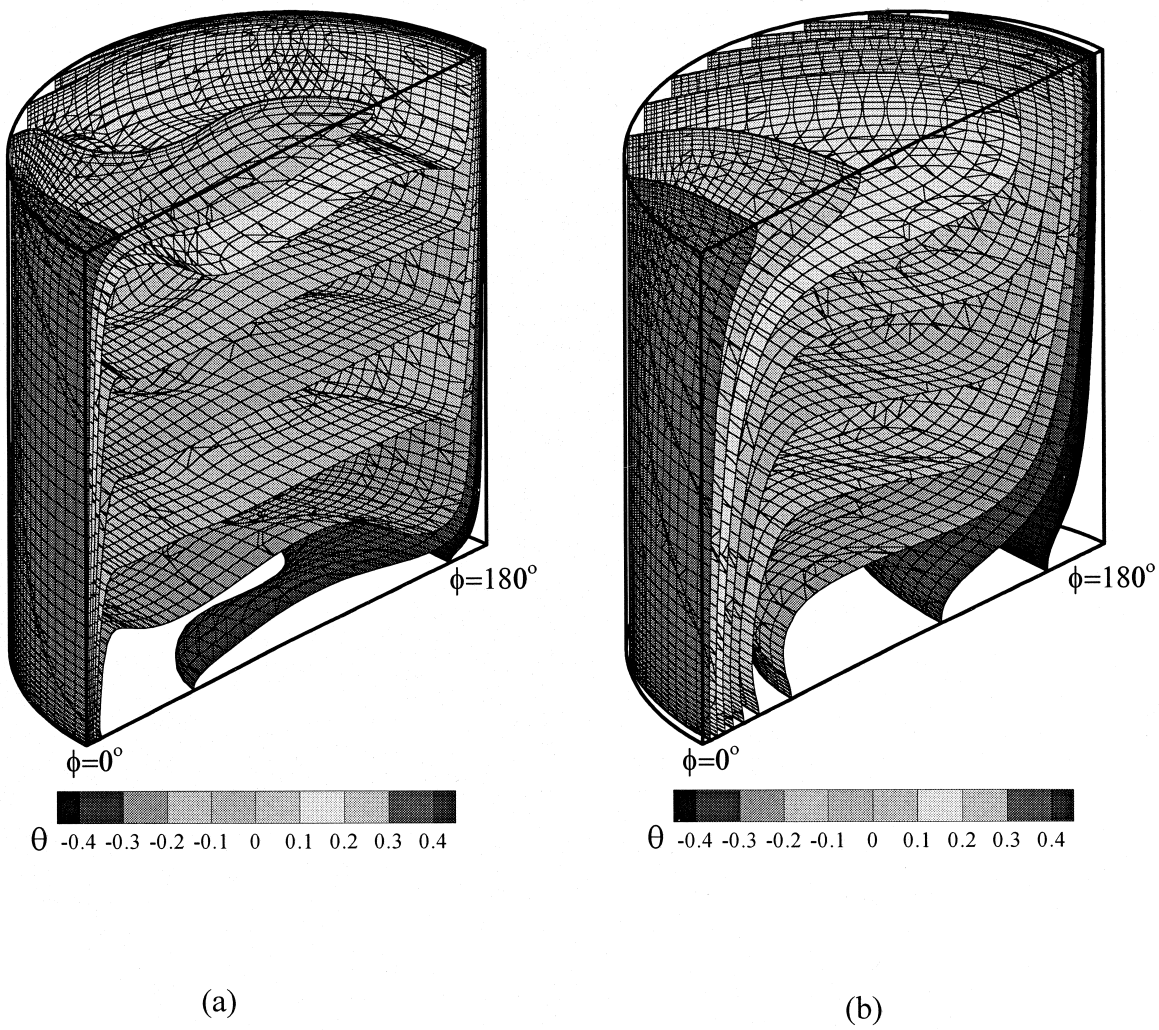

Fig. 3. Perspective views of isotherms for the standard run. $Pr = 0.71$, $n = 1$, $A = 2$, $S_z = 0$. (a) $Ra = 10^6$; (b) $Ra = 10^4$.

$$U\frac{\partial W}{\partial X} + V\frac{\partial W}{\partial Y} + W\frac{\partial W}{\partial Z} = -\frac{\partial P}{\partial Z} + Pr\nabla^2 W \tag{4}$$

$$U\frac{\partial \theta}{\partial X} + V\frac{\partial \theta}{\partial Y} + W\frac{\partial \theta}{\partial Z} = \nabla^2\theta \tag{5}$$

In the above, nondimensionalization was implemented as follows

$$(X, Y, Z) = \left(\frac{x}{R}, \frac{y}{R}, \frac{z}{R}\right);$$

$$(U, V, W) = \left(\frac{uR}{\alpha}, \frac{vR}{\alpha}, \frac{wR}{\alpha}\right); \quad P = \frac{pR^2}{\rho\alpha^2};$$

$$\theta = \frac{T - T_0}{\Delta T},$$

where $T_0 \equiv (T_{\max} + T_{\min})/2$, and $\Delta T \equiv (T_{\max} - T_{\min})$.

The lower-case symbols refer to the dimensional quantities, and α the thermal diffusivity. The dimensionless parameters are the Rayleigh number $Ra \equiv g\beta\Delta T H^3/\nu\alpha$, the Prandtl number $Pr \equiv \nu/\alpha$, in which ν the kinematic viscosity, and the Boussineq-fluid relationship $\rho = \rho_0[1 - \beta(T - T_0)]$ is adopted. Here, $T_{\max}$ and $T_{\min}$ represent, respectively, the maximum and minimum values of temperature that are specified at the boundary wall at the same height, say, at $Z = A/2$.

In accordance with the problem statement, the appropriate boundary conditions are

$$U = V = W = 0, \frac{\partial \theta}{\partial Z} = 0 \quad \text{at } Z = 0, A \tag{6}$$

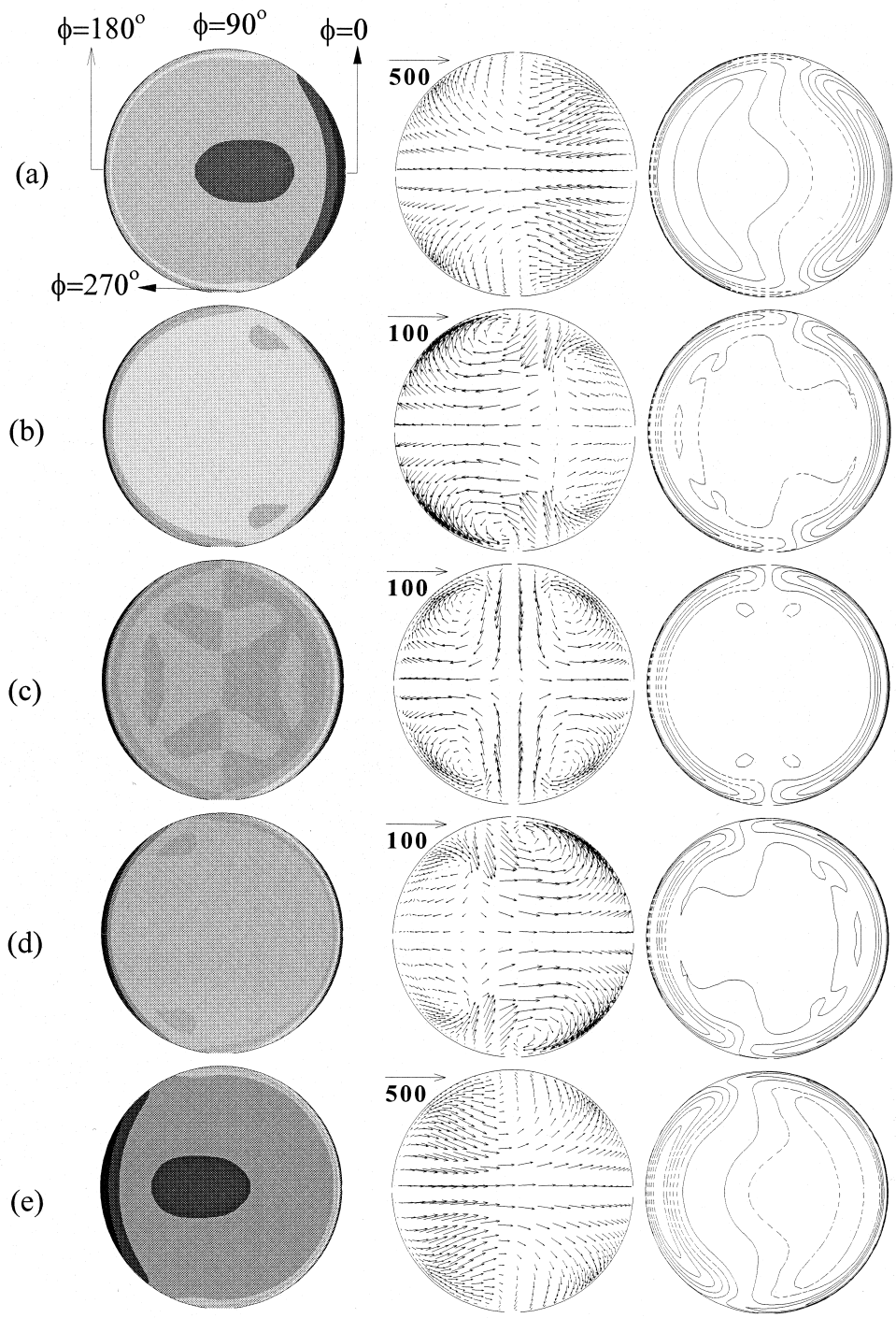

Fig. 4. Temperature and velocity fields in constant-height planes for the standard run. $S_z = 0$. The left column indicates temperature (θ), the middle column horizontal velocities, and the right column vertical velocities. The vertical locations are: (a) $Z = 1.9$; (b) $Z = 1.5$; (c) $Z = 1.0$; (d) $Z = 0.5$; (e) $Z = 0.1$.

$$U = V = W = 0, \theta_\Sigma = \frac{1}{2}\cos(n\phi) + f(Z),\ f(Z) = (Z/A - 1)S_z \text{ at the vertical sidewall} \tag{7}$$

The sidewall temperature condition, θ_Σ in Eq. (7), drives the buoyant convection in the cylinder. As is apparent, $f(Z)$ and $\cos(n\phi)$ indicate the vertical and azimuthal variations of the imposed sidewall temperature, respectively. It is important that $f(Z)$ is an increasing function with Z, and ϕ denotes the azimuthal angle. Clearly, the severity of the azimuthal inhomogeneity of θ_Σ is represented by the index n. Also, the vertical profile of θ_Σ is linear with height if $S_z = 1.0$, and a nonlinear variation of θ_Σ with height can be modeled by adjusting $S_z = S_z(Z)$.

The use of Cartesian coordinates, instead of a cylindrical frame, needs some explanation. As is well known, if a cylindrical frame is adopted, special techniques have to be utilized to overcome the computational singularity at the axis (see, e.g., [18]). Furthermore, a large number of grid points will have to be placed in the vicinity of the axis. In the present problem, flow details near the axis are not of primary concern; therefore, such a concentration of grid points in the neighborhood of the axis is not desirable. Based on these considerations, the straightforward Cartesian coordinates are selected. As remarked, the purpose of this study lies in gaining an understanding of the physical aspects of flow, rather than in developing numerical methodologies.

Fig. 2 exemplifies the grid network in the x–y plane. The grids are indexed by choosing four corners ($\phi = 45^\circ$, 135°, 225° and 315°) on the periphery. The present grid generation method stems from the Thomas–Middlecoff scheme [19] and the suggestions of Ref. [20]. By undergoing a series of trials, the present grid organization has been tested to perform effectively with a high degree of accuracy. Grid stretching was also deployed in the vertical direction. For most calculations, the typical grid used was ($52 \times 52 \times 52$). For several sample runs, extensive grid-convergence tests were conducted. Four different meshs, i.e., ($32 \times 32 \times 32$), ($42 \times 42 \times 42$), ($52 \times 52 \times 52$) and ($62 \times 62 \times 62$) were employed to compute the exemplary case of $Ra = 10^6$, $A = 2.0$, $Pr = 0.71$. The computed velocity field demonstrated a high degree of grid-independence between the ($52 \times 52 \times 52$) and ($62 \times 62 \times 62$) meshs. Similar trends were monitored in other sample calculation runs.

Numerical solutions to the above equations were acquired by using the well-documented SIMPLE algor-

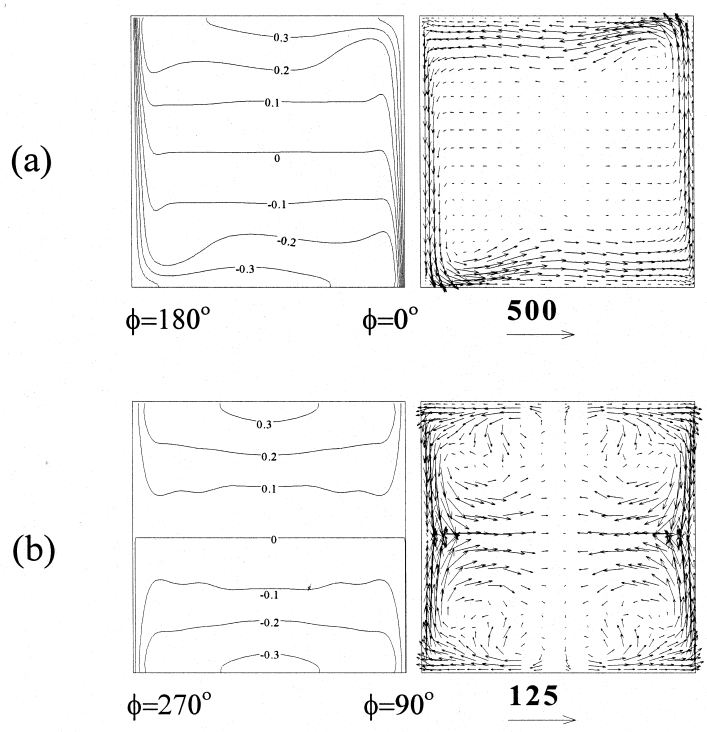

Fig. 5. Flow in the axial planes. $S_z = 0$. (a) The plane linking $\phi = 0^\circ$ and $\phi = 180^\circ$; (b) the plane linking $\phi = 90^\circ$ and $\phi = 270^\circ$. The left column indicates temperature (θ), and the right column velocities in the axial plane.

ithm [21]. The general cartesian coordinates were utilized, and the numerical procedures followed Peric [20]. The nonlinear terms were discretized by employing the QUICK scheme [22], which is known to enhance accuracy. In order to solve the discretized pressure equation, the CGS solver [23] was adopted, and for other dependent variables, the SIP solver [24] was selected. Convergence was declared when the relative differences in nondimensional velocity and temperature fields fell below 10^{-4}.

With a view toward establishing the robustness of the numerical methodology, a variety of benchmark testings were carried out, and cross-comparisons were made of the average Nusselt numbers at the vertical walls of a differentially-heated cubical enclosure. Furthermore, for buoyant convection in a horizontal cylinder, the maximum values of velocity components were compared between the results of [15] and the present calculations. These results were highly consistent and mutually-supportive. These validation efforts gave credence to the reliability and accuracy of the numerical solution procedures of the present paper.

3. Results and discussion

The mission here is to isolate the effect of the horizontal variation of temperature at the sidewall on the resulting three-dimensional buoyant flow. For this purpose, a standard set of parameter values is chosen: $Ra = 10^6$, $Pr = 0.71$, $A = 2.0$, $S_z = 0.0$ and $n = 1$. The value of Ra ($=10^6$) is considered to be sufficiently large to render a boundary layer-type flow, and air ($Pr \cong 0.71$) was selected for the fluid. The parameter $n = 1$ implies that, as seen in Eq. (7), the sidewall temperature variation has a wavelength of the entire circumference of the cylinder. Also, in this standard case, the sidewall temperature is uniform in the vertical direction [$S_z = 0.0$].

Fig. 3 demonstrates the perspective views of isotherm surfaces in the cylinder. For comparison purposes, the case of $Ra = 10^4$ is also included. For the standard run ($Ra = 10^6$), Fig. 3(a) exhibits the eminent characteristics of three-dimensional buoyant convection. The azimuthal angles for the cut axial plane displayed in Fig. 3 are $\phi = 0^\circ$ (corresponding to the location of T_{max}) and $\phi = 180^\circ$ (T_{min}), respectively. For the case of $Ra = 10^6$, a distinct boundary layer is seen, and in the bulk of the interior, the isotherm surfaces are nearly horizontal. Clearly, for the case of $Ra = 10^4$, as illustrated in Fig. 3(b), the thickness of boundary layer is larger than that of $Ra = 10^6$; furthermore, the division of the flow field into the boundary layer and interior is less distinct. It is also evident that, for $Ra = 10^4$, due to the comparatively greater

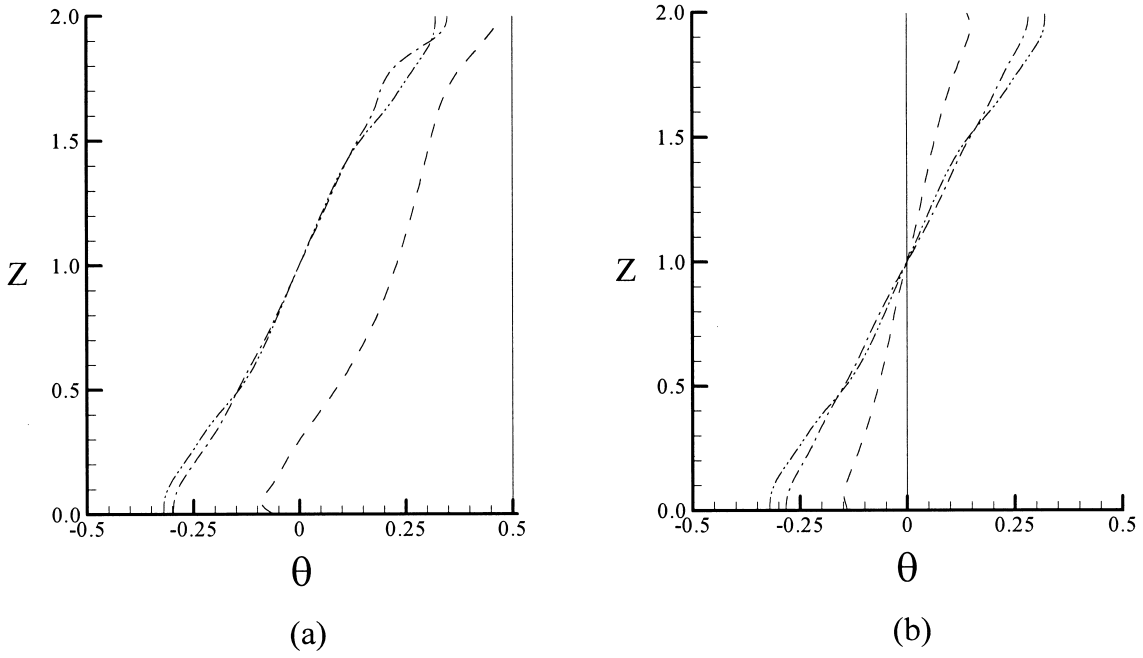

Fig. 6. Vertical profiles of temperature. $S_z = 0$. (a) $\phi = 0^\circ$, (b) $\phi = 90^\circ$. The radial locations are: ———, $r/R = 1.0$ (wall); – – – – –, $r/R = 0.95$; ·····, $r/R = 0.50$; –·–·–·–, $r/R = 0.0$.

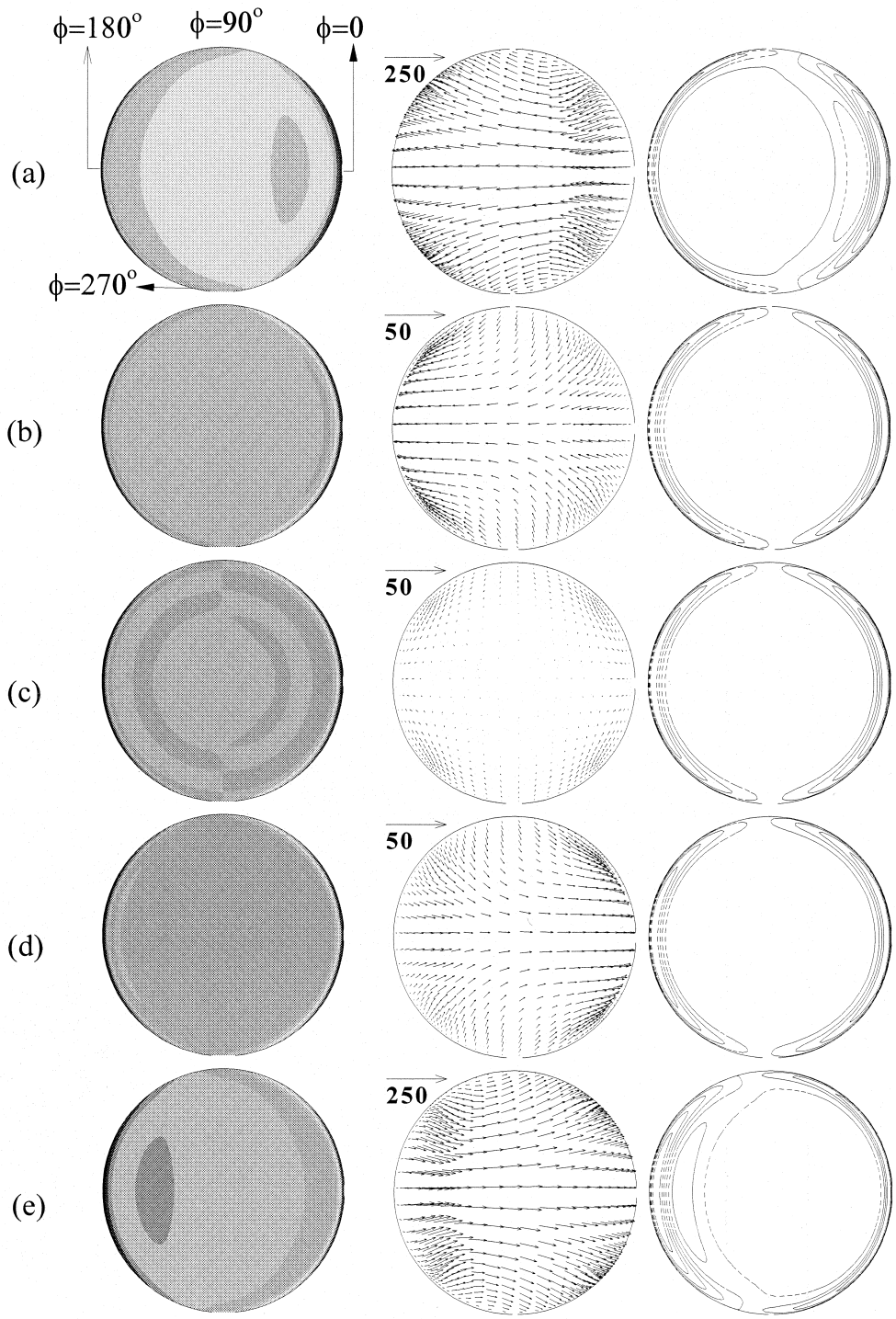

Fig. 7. Temperature and velocity fields in constant-height planes for the standard run. $S_z = 1.0$. The left column indicates temperature (θ), the middle column horizontal velocities, and the right column vertical velocities. The vertical locations are: (a) $Z = 1.9$; (b) $Z = 1.5$; (c) $Z = 1.0$; (d) $Z = 0.5$; (e) $Z = 0.1$.

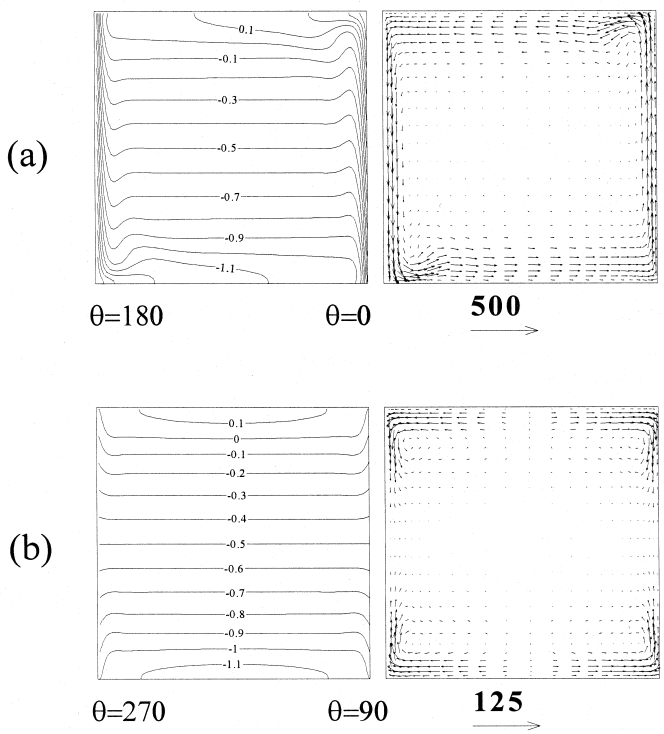

Fig. 8. Flow in the axial planes. $S_z = 1.0$. (a) The plane linking $\phi = 0^\circ$ and $\phi = 180^\circ$; (b) the plane linking $\phi = 90^\circ$ and $\phi = 270^\circ$. The left column indicates temperature (θ), and the right column velocities in the axial plane.

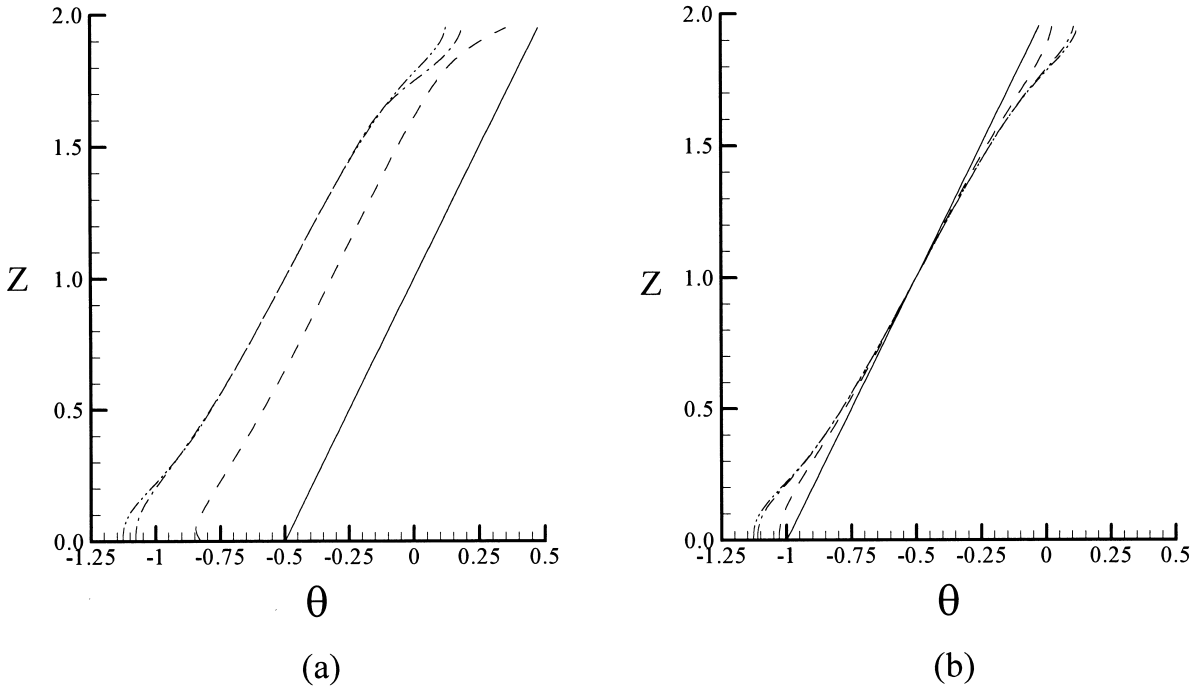

Fig. 9. Vertical profiles of temperature. $S_z = 1.0$. (a) $\phi = 0^\circ$, (b) $\phi = 90^\circ$. The radial locations are: ———, $r/R = 1.0$ (wall); – – – – – $r/R = 0.95$; ·····, $r/R = 0.50$; —·—·—·—, $r/R = 0.0$.

influence of conduction, the deviations of the isotherm surfaces in the interior from the horizontal plane are larger than for $Ra = 10^6$. A general observation can be made in the global temperature field. The isotherm surfaces show *S*-shaped patterns near the wall, which are caused by the rising (sinking) motion in the vicinity of $\phi = 0^\circ$ ($\phi = 180^\circ$) regions. These fluid motions turn into horizontal flows near the top and bottom insulated walls.

The detailed velocity structure for the standard run is plotted in Fig. 4. The three components of velocity in the horizontal cut planes are shown. It is significant to note that the azimuthal variation of the boundary temperature is largely absorbed in the boundary layer and that a uniform temperature prevails in much of the interior region. The temperature variation at the wall does not penetrate into the interior region, and the temperature in the interior responds to the average of the wall temperature. This qualitative assertion was made by Jischke and Doty [11], and the present numerical results are consistent with this ascertainment.

The horizontal flows are concentrated in the boundary layers near the horizontal endwalls (see rows (a) and (e) of Fig. 4). In the top boundary layer (see row (a) of Fig. 4), the horizontal flows in the central portions are generally from the hot side (near $\phi = 0^\circ$) toward the cold side (near $\phi = 180^\circ$), and the circuit is closed by forming two circulation cells, i.e., one each in the top and bottom hemisphere. In the bulk of interior (see rows (b), (c) and (d) of Fig. 4), the horizon-

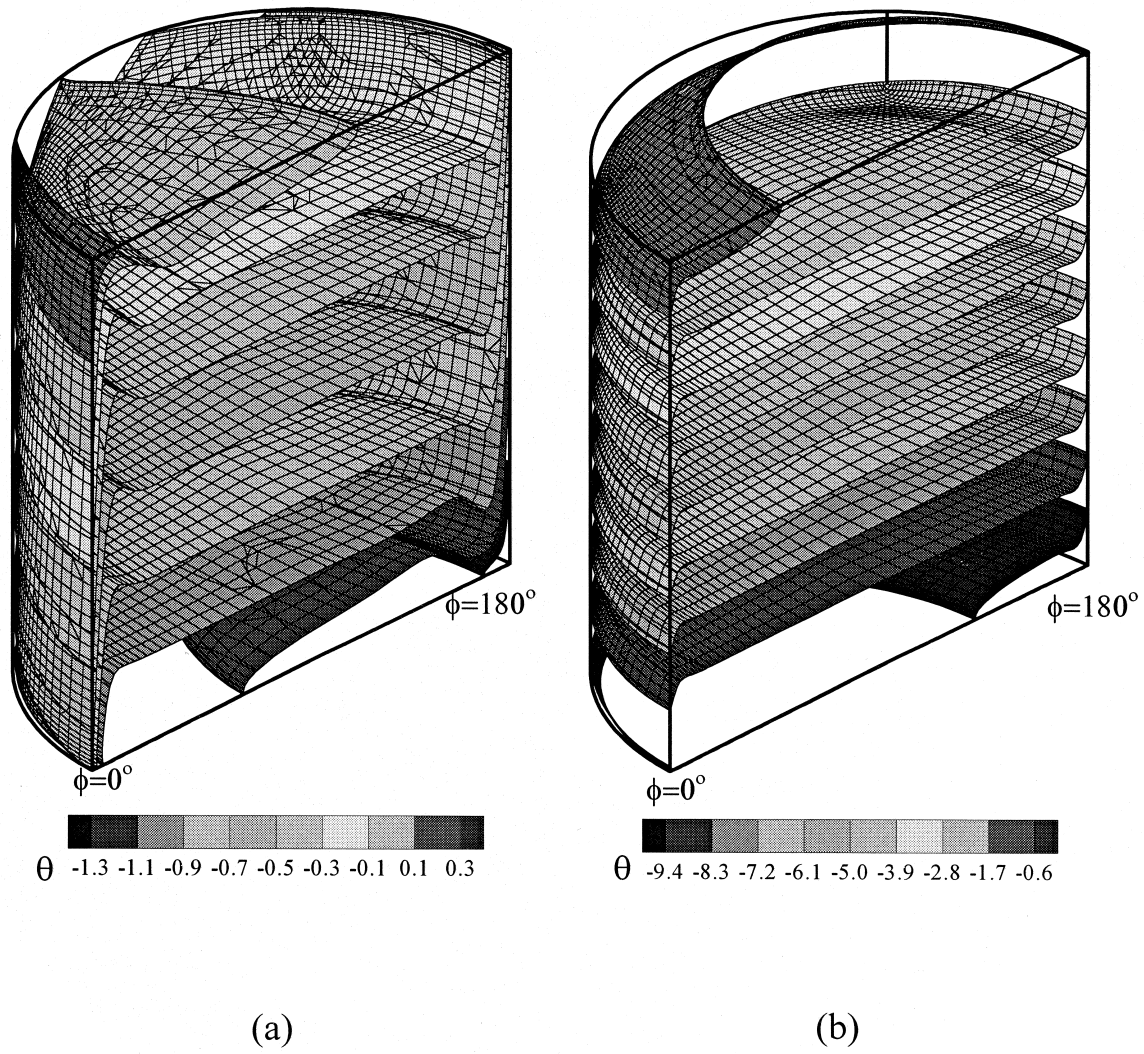

Fig. 10. Perspective views of isotherm surfaces. $Ra = 10^6$, $Pr = 0.71$, $n = 1$. (a) $S_z = 1.0$; (b) $S_z = 10.0$.

tal flows are weak (note the difference in scales for the plots of horizontal velocities in Fig. 4). The horizontal velocities in the interior sections of the cylinder display rather complex patterns (see rows (b), (c) and (d) of Fig. 4). Near the mid-height (see row (c) of Fig. 4), the horizontal flows in the y-direction appear along the diameter linking $\phi = 90^\circ$ and $\phi = 270^\circ$, and the overall patterns of horizontal flows constitute four cells. The horizontal flows originate from the regions of $\phi = 90^\circ$ and $\phi = 270^\circ$, move toward the center of the horizontal plane, and then diverge toward the hot ($\theta = 0^\circ$) and cold ($\theta = 180^\circ$) wall regions.

The results for the vertical velocity are informative. In contrast to the horizontal velocities, the vertical velocity is greatest near the mid-height, and it decreases as the location moves close to the horizontal endwalls. In general, the vertical velocities are concentrated to the boundary layers, and in much of the interior, the vertical flows are negligibly small. As clearly exhibited in Fig. 4, in large portions of the boundary layer surrounding the hot (cold) side, the vertical flow is upward (downward). The present description of the global picture of vertical flows is in qualitative accord with the previous analytical studies [11].

Flow variables in the axial planes are displayed in Fig. 5 for the standard case ($S_z = 0$). The flow pattern in the axial plane linking the hot ($\phi = 0^\circ$) and cold regions ($\phi = 180^\circ$) is qualitatively akin to that of the benchmark two-dimensional cavity flow. A single counterclockwise circulating cell is visible, and, as expected, flow is very weak in the interior core. In the neutral axial plane cutting through $\phi = 90^\circ$ and $\phi = 270^\circ$, due to symmetry, vertical velocities vanish at the mid-height of the cylinder. This creates a four-cell structure, as is discernible in Fig. 5(b), and the overall magnitudes of velocities are very small. Throughout the entire flow region, the fluid is stably-stratified in the bulk of the interior region.

In an effort to delineate the thermal response of the interior region, the vertical profiles of temperature at various radial positions are exhibited in Fig. 6 for $S_z = 0$. Clearly, at $\phi = 0^\circ$, the wall temperature is highest ($\theta = 0.5$) and vertically uniform. However, due to buoyant convective activities, both in the boundary layer region ($r = 0.95$) and in the interior core, the fluid develops stratification. Also, at the neutral circumferential angle ($\phi = 90^\circ$), the wall temperature is uniformly zero. However, the prevailing fluid stratification in the interior is manifested.

Next, the case of $S_z = 1.0$ in Eq. (7) is considered. This indicates that the imposed temperature at the cylindrical wall increases with height, which creates a stably-stratified boundary condition from the outset. The solutions viewed in constant-height planes are exhibited in Fig. 7. In comparison to the results for $S_z = 0$ in Fig. 4, the velocities for $S_z = 1.0$ are generally smaller in magnitude (note the difference in scales used in Figs. 4 and 7). These plots illustrate that flows are reduced in strength as the imposed stratification inhibits vertical motions. In particular, horizontal velocities in the vicinity of the cylinder mid-height become very small. Near the top endwall, the horizontal flows move to the left from the hot to the cold regions. Near the bottom endwall, the situation is opposite to that near the top endwall. As clearly demonstrated in Fig. 7, the fluid temperature in the horizontal planes in the interior core is largely uniform, and the temperature nonuniformities forced at the cylindrical wall are absorbed in the thin boundary layers. As stressed earlier, the fluid in the interior core responds to the horizontally-averaged value of the temperature imposed on the surface of the container.

The axial-plane plots for $S_z = 1.0$ are shown in Fig. 8. The attenuation of velocities is evident. Also, a strong vertical stratification is developed in the interior, which is caused by the imposed temperature distribution at the wall. In comparison to the case of $S_z = 0$, the results for $S_z = 1.0$ indicate that all three velocity components are reduced in magnitude and they tend to be confined to thin boundary layers near the cylindrical wall.

The vertical profiles of temperature for $S_z = 1.0$ are displayed in Fig. 9. At the azimuthal position corresponding to the hot point ($\phi = 0^\circ$), the vertical gradients of temperature in the interior are substantially the same as that on the wall. The values of temperature themselves are lower than that at the wall due to the fluid motions in the cylinder. At the neutral azimuthal

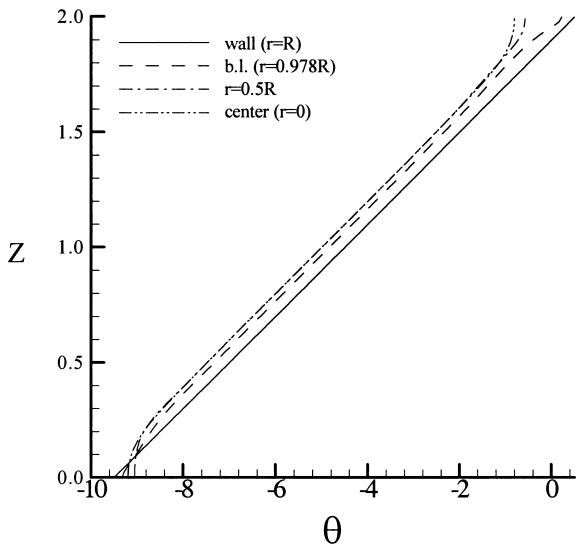

Fig. 11. Variation of temperature with height at $\phi = 0^\circ$. $S_z = 10.0$.

position ($\phi = 90^\circ$), both the gradients and magnitudes of temperature in the interior are very close to those at the wall.

The results for larger values of S_z are scrutinized. The perspective views of temperature fields are portrayed in Fig. 10 for S_z = 1.0 and 10.0. Clearly, as S_z increases, the stable stratification in the fluid interior is distinct and the isotherms are highly flat and horizontal in wider regions of the interior. Also, the vertical temperature profiles along a radial cut ($\phi = 0^\circ$) for S_z = 10.0 are displayed in Fig. 11. Cross-comparisons of the results in Figs. 6(a), 9(a) and 11 are revealing. When S_z is large, the fluid in the entire domain, both in the boundary and the interior, develops the vertical temperature distribution which is very close to the imposed sidewall temperature profile.

4. Conclusions

The computed results for three-dimensional buoyant flows are summarized below.

When θ_Σ is vertically uniform, the azimuthal variation of the wall temperature is absorbed in the boundary layer. The interior core is stably stratified with horizontal isotherms. In the horizontal planes, the fluid moves from the hot to the cold regions, forming two circulation cells near the endwall zones. Near the mid-height, due to symmetry, the horizontal motions produce a four-cell structure. In the axial planes linking $\phi = 0^\circ$ and $\phi = 180^\circ$, a single cell is visible; however, in the neutral axial plane linking $\phi = 90^\circ$ and $\phi = 270^\circ$, four cells are manifested.

When θ_Σ increases with height, the interior fluid motions are reduced in magnitude. The interior core is strongly stratified. The velocity patterns in the horizontal planes and in the axial planes are characteristic of a stratified flow. The vertical gradients of temperature in the interior become closer to that on the surface wall. As S_z increases, broader regions of the interior have a distinct and stable stratification. The vertical temperature profiles in the interior domain become similar to the imposed boundary wall temperature distributions.

Acknowledgements

This work was supported in part by a Guest Professorship to JMH at Kyushu University. Support was also provided by AFERC (Pohang), KOSEF-RRC (Sun Moon University), and the R&D Management Center for Energy and Resources, South Korea.

References

[1] G. de Vahl Davis, Natural convection of air in a square cavity: a benchmark numerical solution, International Journal for Numerical Methods in Fluids 3 (1983) 249–264.
[2] T. Fusegi, J.M. Hyun, Laminar and transitional natural convection in an enclosure with complex and realistic conditions, International Journal of Heat and Fluid Flow 15 (4) (1994) 258–268.
[3] G.D. Mallinson, G. de Vahl Davis, Three-dimensional natural convection in a box: a numerical study, Journal of Fluid Mechanics 83 (1) (1977) 1–31.
[4] T. Fusegi, J.M. Hyun, A numerical study of 3D natural convection in a cube: effects of the horizontal thermal boundary conditions, Fluid Dynamics Research 8 (1991) 221–230.
[5] T. Fusegi, J.M. Hyun, K. Kuwahara, B. Farouk, A numerical study of three-dimensional natural convection in a differentially heated cubical enclosure, International Journal of Heat and Mass Transfer 34 (6) (1991) 1543–1557.
[6] T. Tagawa, H. Ozoe, Enhanced heat transfer rate measured for natural convection in liquid gallium in a cubical enclosure under a static magnetic field, ASME Journal of Heat Transfer 120 (1998) 1027–1032.
[7] M. Akamatsu, K. Kakimoto, H. Ozoe, Numerical computation for the secondary convection in a Czochralski crystal growing system with a rotating crucible and a static crystal rod, Journal of Materials Processing & Manufacturing Science 5 (1997) 329–348.
[8] K. Toh, H. Ozoe, Dopant concentration profile in a Czochralski flow of liquid metal in a vertical or a horizontal magnetic field, Journal of Crystal Growth 130 (1993) 645–656.
[9] T.H. Kuehn, R.J. Goldstein, An experimental and theoretical study of natural convection in the annulus between horizontal concentric cylinders, Journal of Fluid Mechanics 74 (4) (1976) 695–719.
[10] C. Kleinstreuer, M. Lei, Transient buoyancy-induced three-dimensional flows in slender enclosures with coaxial heated cylinder, International Journal of Engineering Science 32 (10) (1994) 1635–1646.
[11] M.C. Jischke, R.T. Doty, Linearized buoyant motion in a closed container, Journal of Fluid Mechanics 71 (4) (1975) 729–754.
[12] E. Crespo, D. Arco, P. Bontoux, Numerical solution and analysis of asymmetric convection in a vertical cylinder: an effect of Prandtl number, Physics of Fluids A1 (8) (1989) 1348–1359.
[13] H. Potts, W.R. Wilcox, Thermal fields in the Bridgman–Stockbarger technique, Journal of Crystal Growth 73 (1985) 350–358.
[14] G.T. Neugebauer, W.R. Wilcox, Convection in the vertical Bridgman–Stockbarger technique, Journal of Crystal Growth 89 (1988) 143–154.
[15] J.P. Pulicani, J. Ouazzani, A Fourier–Chebyshev psedospectral method for solving steady 3-D Navier–Stokes and heat equations in cylindrical cavities, Computers Fluids 20 (2) (1991) 93–109.
[16] J.P. Pulicani, S. Krukowski, J. Iwan, D. Alexander, J.

Ouazzani, F. Rosenberger, Convection in an asymmetrically heated cylinder, International Journal of Heat and Mass Transfer 35 (9) (1992) 2119–2130.

[17] Y.H. Li, K.C. Lin, T.F. Lin, Computation of unstable liquid metal convection in a vertical closed cylinder heated from the side and cooled from above, Numerical Heat Transfer Part A 32 (1997) 289–309.

[18] H. Ozoe, K. Toh, A technique to circumvent a singularity at a radial center with application for a three-dimensional cylindrical system, Numerical Heat Transfer Part B 33 (1998) 355–365.

[19] P.D. Thomas, J.F. Middlecoff, Direct control of the grid point distribution in meshes generated by elliptic equations, AIAA Journal 18 (1980) 626–656.

[20] M. Peric, Finite volume method for the prediction of three-dimensional fluid flow in complex ducts, PhD thesis, Imperial college, London, 1985.

[21] S.V. Patankar, Numerical Heat Transfer and Fluid Flow, MacGraw-Hill, New York, 1980.

[22] B.P. Leonard, A stable and accurate convection modeling procedure based on quadratic upstream interpolation, Computer Methods in Applied Mechanics and Engineering 19 (1979) 59–98.

[23] P. Sonneveld, CGS: a fast Lanczos type solver for nonsymmetric linear systems, SIAM Journal on Sci. Stat. Comput 10 (1989) 36–52.

[24] H.L. Stone, Iterative solution of implicit approximations of multidimensional partial difference equations, SIAM Journal on Numerical Analysis 5 (1968) 530–558.